



Suppression of humping bead in high-speed triple-wire gas indirect arc welding

Zeli Wang¹ · Tianyi Zhang¹ · Xiaonan Dong¹ · Liming Liu¹

Received: 18 March 2022 / Accepted: 22 August 2022 / Published online: 7 September 2022
© The Author(s), under exclusive licence to Springer-Verlag London Ltd., part of Springer Nature 2022

Abstract

Triple-wire gas indirect arc welding (TW-GIA) is a new technology with the advantages of low heat input and high deposition rate. However, the humping bead restricts the improvement of welding efficiency. In this article, the high-speed cameras and infrared thermal imaging system were used to characterize the formation mechanism of the TW-GIA humping bead. The physical model was established to discuss the force mechanism of the weld pool. And the influence of process parameters on humping bead was studied. The results show that the increase of the welding angle reduced the arc pressure and droplet impact force in the opposite direction of welding, which was beneficial to eliminate the hump. When the welding height was lower than 3 mm, the excessive arc pressure led to the humping bead with arc crater. When the welding height was greater than 20 mm, the distance between the droplets of side wires was far, forming the humping bead with “double bead” defect. In addition, the flow distance of the liquid metal shortened as the welding current decreased, which could suppress the humping bead. When the ratio of the total wire feeding speed to the welding speed was 10, the critical current was 360 A, and the critical current increased as the ratio increased. The maximum TW-GIA welding speed of bead-on-plate was 4.2 m/min, which was 137% higher than that of high-speed GMAW.

Keywords Triple-wire gas indirect arc welding · Humping bead · Welding efficiency · Force mechanism · Process parameters

1 Introduction

With the increase in market demand, methods to improve welding efficiency have become the focus of modern industrial research. Increasing deposition rate to reduce welding time is the most direct method [1–3]. For example, Tandem welding [4, 5] utilizes two wires to melt synchronously, which significantly improves welding efficiency. T.I.M.E welding [6, 7] increases the allowable current by changing the gas composition, and it has been proven that the deposition rate can reach triple times that of the traditional gas metal arc welding (GMAW) [8]. However, the prerequisite for these technologies to increase deposition rate is to increase the welding current. The heat input of base metal increases accordingly, which is prone to defects such as

undercut [9] and welding deformation [10]. Bypass coupled arc welding [11–13] allows part of the welding current to pass through the auxiliary wire and the rest to pass through the base metal. This achieves the effect of increasing deposition rate and reducing heat input. To further reduce heat input, the twin-wire indirect arc welding (TWIAW) [14, 15] uses the method of separating the base metal from electrode. The positive and negative electrodes of the power are connected by two independent wires, so that the current does not flow through the base metal. The heat-carrying mechanism of base metals is changed to realize the decoupling effect of heat input and deposition rate. However, due to the asymmetrical spatial distribution of the magnetic field, the arc diverges seriously under large welding current. The adjustment of process parameters needs to be very precise, which increases the difficulty of the welding process [16].

Recently, a new high-efficiency welding technology called triple-wire gas indirect arc welding (TW-GIA) has been proposed [17]. In this technology, two indirect arcs are generated between the wires and are coupled into one body in space. The symmetrical space magnetic field enables the

✉ Liming Liu
liulm@dlut.edu.cn

¹ Liaoning Key Laboratory of Advanced Welding and Joining Technology, Dalian University of Technology, Dalian 116024, China

arc to withstand large welding current and is more tolerant to small error of process parameter adjustment. Liu et al. [18] explored the process parameter range of TW-GIA, and results show allowable current could reach more than 480 A (twice of TWIAW). Due to the expansion of the process parameter range, TW-GIA solved the sidewall non-fusion defect that appears in the thick plate welding process of TWIAW [19]. However, the special metal transfer and weld pool flow characteristics make it prone to humping bead when the welding speed exceeds 2.8 m/min, which severely restricts the further improvement of TW-GIA welding efficiency [20].

At this stage, the causes and suppression measures of humping bead in arc welding have been deeply discussed. Wang et al. [21] proposed that the main reason for the formation of humping bead was capillary instability caused by surface tension. Nguyen et al. [22] believed that the high momentum reverse liquid metal flow in the weld pool was the main cause of the humping bead. Zahr et al. [23] explored the influence of shielding gas composition on TIG welding hump, and found that adding helium gas increased the heat transfer to the workpiece, thereby slowing down the occurrence of hump defects and increasing the welding speed. Li et al. [24] used double-electrode welding to distribute the arc pressure over a wider area, resulting in weakening of the surface depression of the weld pool. This reduced the kinetic energy of the metal liquid flowing in the reverse direction and eliminated the hump defect. Kanemaru et al. [25] adopted a TIG-MAG hybrid welding, which improved the heat transfer of the weld pool, so that the momentum of the liquid metal flowing in the reverse direction was reduced, and the occurrence of hump defects was suppressed. Shoichi et al. [26] used an upward electromagnetic force to lift the molten metal up in flat hot wire TIG welding with excessive heat input, and the hump defect was significantly suppressed. Wu et al. [27] and Wang et al. [28] applied an external

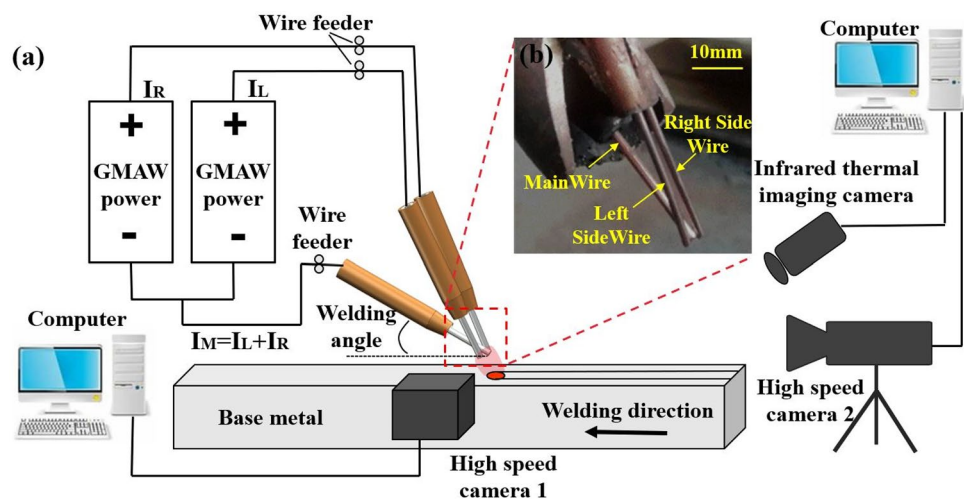
transverse magnetic field to the weld pool to control the behavior of the liquid metal, and successfully prevented the weld bulge. Gatzen et al. [29] used a coaxial magnetic field to control the flow of molten metal through electromagnetic stirring. Experiments and numerical simulations show that both the frequency of the magnetic field and the magnetic flux density had an effect on the distribution and concentration of the elements. Bachmann et al. [30] used a stable magnetic field to reduce the flow rate through the Hartmann effect in the partial penetration laser welding of thick aluminum parts, and eliminated the humping bead caused by the hot capillary flow.

However, the TW-GIA current forms a loop between the three wires, and the three wires melted simultaneously, which increases the complexity of the droplet behavior. In addition, since the base metal is separated from the electrode, the heating mechanism of the base metal and the flow characteristics of the weld pool are changed from the traditional arc welding. So, the existing experience of eliminating the hump cannot be completely used for reference. This article aims to clarify the formation mechanism of TW-GIA humping bead and improve welding efficiency. The high-speed cameras and infrared temperature measurement system were used to record the flow status of the TW-GIA molten metal. The physical model was built to discuss the force of the weld pool. And the influence of welding angle, welding height, and welding current on humping bead was analyzed. It is of practical significance to promote the market application of TW-GIA.

2 Experimental system

Figure 1 is a schematic diagram of the experimental equipment. The TW-GIA welding system is mainly composed of two welding power sources and three independent wire

Fig. 1 Schematic diagram of experimental equipment: **a** overall schematic diagram of the equipment, **b** detail of the wires arrangement



feeding mechanisms. The three wires are arranged as shown in Fig. 1b. The middle wire is called the main wire, and the other two wires are called the left side wire and the right side wire according to their positions. The positive poles of the two welding power sources are respectively connected to the two side wires, and the negative poles are concentrated on the main wire. Therefore, the current formed a loop between the three wires, the main wire current $I_M = I_L + I_R$, I_L , and I_R are the left and right side wire currents respectively, and the welding current referred to in this article is the main wire current. The three wires are in point contact before starting the arc, and the welding height is the distance between the wires intersection point and the base metal. When starting the arc, the two power sources are turned on synchronously so that the current formed a loop between the three wires, and the resistance heat and arc heat melt the continuously fed wires. The base metal is placed on the platform of the FLS40 orbital moving system produced by Chengdu FUYU Technology Company. The system has manual and automatic operation functions. In the experimental preparation stage, in order to avoid metal bumps at the beginning of the weld bead, the base metal is farther away from the welding torch. By setting the running speed and running direction of the moving system, the base metal moves in accordance to the predetermined welding direction during the arc stabilization stage to start the welding process.

Two welding modes are used: bead-on-plate welding and butt welding. The purpose of butt welding is to demonstrate the practicality of the technique. However, in butt welding, because the liquid metal is in the gap between the base metals, the complete behavior of the liquid is difficult to be captured by the high-speed camera, so the bead-on-plate welding is used to completely present the behavior of the liquid metal with different process parameters, so that the influencing mechanism can be more intuitively discussed. Q345 steel plates with a size of 500 mm × 160 mm × 3.8 mm is adopted as base metal in two modes. The surface of the base metal is polished with a fine wire brush and wiped with acetone and alcohol to remove rust and oil stains. In butt welding, the welding gap is 2.5 mm (two independent base metals with the above size), and ceramic gasket on the back is used to constrain the weld pool. The type of welding wire is ER50-6, the diameter of the main wire and the side wire is 1.6 mm and 1.2 mm respectively, and the extension of the wires is 15 mm. The angle between the side wire and the base metal is fixed at 80°, and the angle between the main wire and the base metal is defined as the welding angle.

Table 1 shows the chemical composition of wire and base metal. The shielding gas composition is 80% Ar and 20% CO₂, and the gas flow rate is 20 L/min.

Two MS50K high-speed cameras produced by Canadian Mega-speed company are placed perpendicular and parallel to the welding direction to record the droplet behavior, with a maximum resolution of 1280 × 1024 and a spectral range of 400–1000 nm. Acquired 2000 pictures per second, with an exposure time of 500 μs. The camera lens added a narrow-band filter with a center wavelength of 659.5 nm to reduce the influence of light of other wavelengths on the captured image. The half-wave bandwidth is 9.4 nm and the peak transmittance is 58.2%. It is worth mentioning that since the time intervals of the key behaviors of hump formation are not consistent, figures of different time intervals have been selected in this paper in order to fully show the details of liquid metal behavior. The SAT-G95 infrared thermal imaging system is used to observe the high temperature area. In order to avoid the overlap of the welding gun on the screen, the angle of the lens and the base material is 70°. According to the pre-experimental debugging, the measuring distance is 1 m, the emissivity is calibrated to 0.84, and the ambient temperature is set to 15 °C.

3 Results and discussion

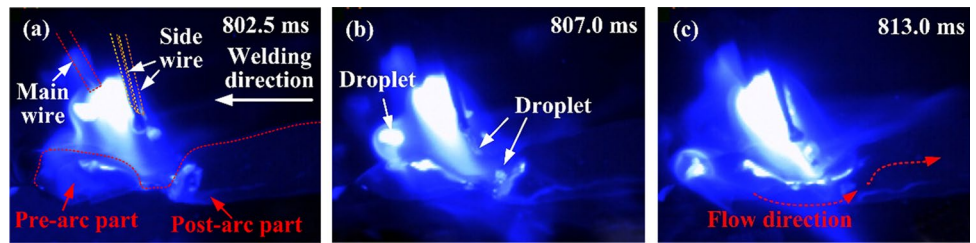
3.1 Formation mechanism of TW-GIA humping bead

The metal transfer and flow state of TW-GIA is different from that of GMAW. Therefore, the cognition of the flow characteristics of the TW-GIA weld pool is the prerequisite for exploring the formation mechanism of the hump. Figure 2 shows the formation process of TW-GIA weld bead. Figure 2a, b shows the droplet transfer process of the two side wires. Figure 2b, c shows the droplet transfer process of the main wire. The transfer frequencies of the side wire droplets and the main wire droplet are different [17], so the delta in time is different. At 802.5 ms (Fig. 2a), the weld pool can be divided into a pre-arc part and a post-arc part. The liquid between the two parts of the weld pool formed a depression under the action of the arc force. In 807.0–813.0 ms (Fig. 2b, c), the droplet of the main wire dripped toward the pre-arc part of the weld pool, and the droplets of the two side wires dripped into the post-arc part. With the movement of the arc, the pre-arc part of the weld pool flowed in the opposite direction of welding to converge

Table 1 Chemical composition (wt.%) of wire and base metal

Materials	C	Mn	Si	S	P	Cu	Fe
Base metal Q345	0.17	1.5	0.5	0.035	0.035	–	Bal
Welding wire ER50-6	0.10	1.54	0.90	0.020	0.018	0.10	Bal

Fig. 2 TW-GIA molten metal flow process: **a** 802.5 ms, **b** 807.0 ms, **c** 813.0 ms



with the post-arc part of the weld pool. Therefore, the pre-arc part of the weld pool is formed by the droplets of the main wire, and the post-arc part of the weld pool is composed of the side wires droplets, the molten workpiece and the transfer liquid from the pre-arc part.

The droplets of the three wires dropped directly into the gap between the two base metals during the TW-GIA butt welding process. Due to the space barrier of the base metals, the high-speed camera cannot capture the entire morphology of the weld pool, so the bead-on-plate welding was used to show the formation details of the typical TW-GIA humping bead. Figure 3 shows the formation process of the humping bead with a welding current of 350 A, welding height of 8 mm, and welding speed of 4.5 m/min. To demonstrate the main steps in a typical hump formation process, figures of irregular time intervals are chosen. In 336.9–405.4 ms (Fig. 3a, b), the main wire droplets and the side wire droplets transferred to the front and back of the arc, respectively. With the movement of the arc in the welding direction, the liquid metal in the pre-arc part was constantly moving in the opposite direction of the welding under the action of the arc force. The large deposition rate of TW-GIA causes metal accumulation far away from the arc. Since the thermal conductivity of metallic solids is much greater than that of air, the weld pool started to solidify from the interface with the base metal. The TW-GIA base metal was separated from the electrode, so the liquid metal far away from the

arc was rapidly cooled under the effect of low heat input [17]. And the fast solidification speed caused the accumulated metal to be constrained by the solidification interface before it was spread. In addition, the solidification interface quickly reached the “valley bottom” in front of the accumulated metal (Fig. 3c), and the upper surface of the valley had received the transfer of the side wire droplets. While the blocking effect of the solid interface caused the counter-flowing liquid metal to accumulate at the front of the interface, unable to fill the valley bottom, and gradually formed the periodic humping bead shown in Fig. 3d. Therefore, the reason for the humping bead is that the low heat input effect of TW-GIA makes the accumulated metal far away from the arc solidify rapidly, which hinders the subsequent metal filling.

3.2 The influence of welding angle on humping bead

Figure 4 shows the TW-GIA butt weld appearance at different welding angle with welding speed of 2.0 m/min, welding current of 380 A, and welding height of 8 mm. When the welding angle was 35°, the weld appearance presented obvious humping bead. When the welding angle was increased to 45°, the volume of the hump was reduced, and the weld appearance was more uniform. When the angle was 55° and 65°, the humping bead disappeared. This indicates that increasing the welding angle is beneficial to eliminate humping bead.

Fig. 3 TW-GIA humping bead formation process: **a** 336.9 ms, **b** 405.4 ms, **c** 579.5 ms, **d** 729.6 ms

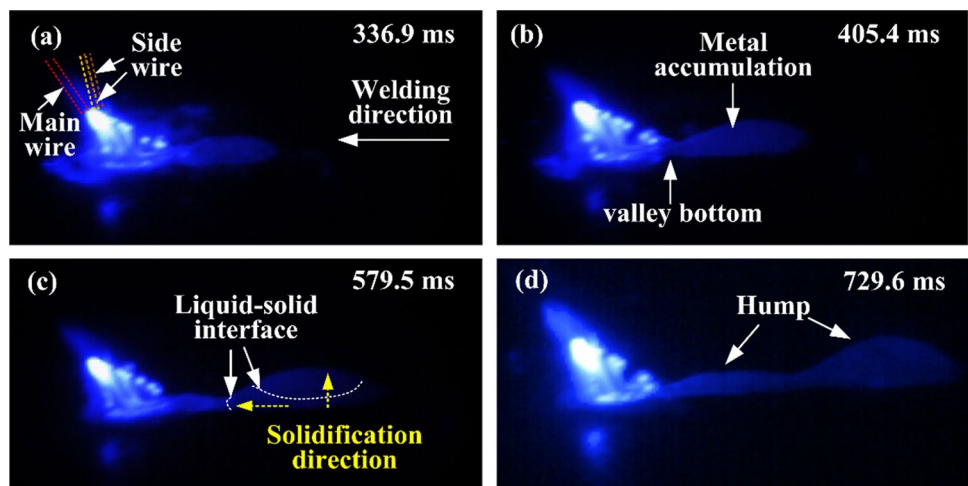
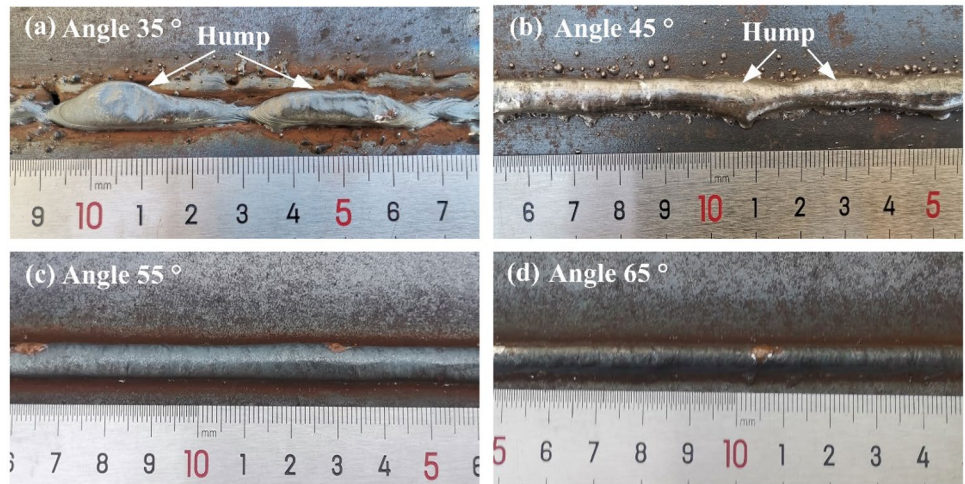


Fig. 4 The appearance of butt welds with different welding angles: **a** welding angle 35°, **b** welding angle 45°, **c** welding angle 55°, **d** welding angle 65°



The conductive channel of the TW-GIA arc was established between the three wires. Therefore, the adjustment of the spatial position of the wires will change the arc shape and droplet transfer behavior, and further influence the flow of the liquid metal. Figure 5 shows the flow process of the weld pool of bead-on-plate welding with welding angles of 35° and 65°. The visual figures captured by the high-speed camera is imported into the AI software, and the distance between the main wire droplet and the side wire droplets can be measured with the diameter of the wires as a reference. When the welding angle was 35°, the transfer distance between the main wire droplet and the side wire droplet was 5.7 mm, and the arc was inclined in the opposite direction of the welding (Fig. 5a). At 170.8 ms, the liquid metal formed a metal accumulation behind the arc. At 301.8 ms, the subsequent metal was not filled to the front of metal accumulation in time. At 415.3 ms, a void was formed at the unfilled position, and the counter-flowing metal accumulated in front of the void to form a humping bead. When the welding angle was 65°, the distance between

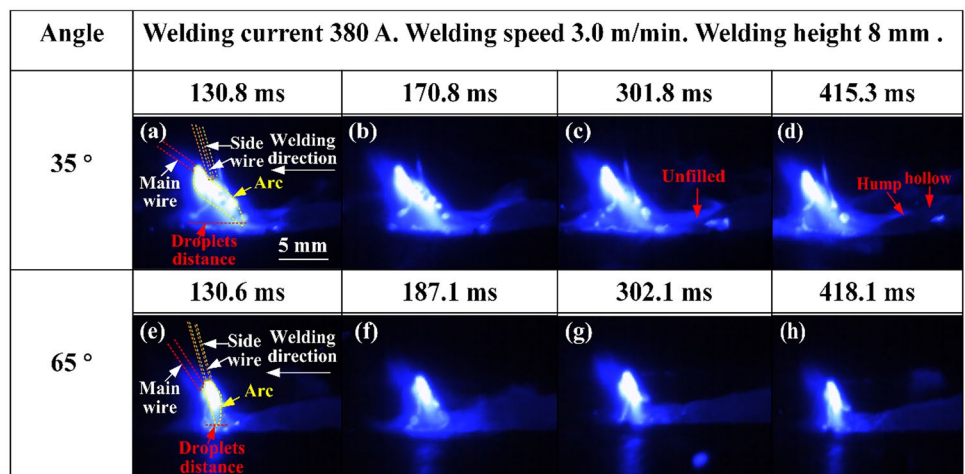
the main wire droplet and the side wire droplet was 2.4 mm. The side wire droplets were almost vertically transferred to the root of the post-arc part of the weld pool, and the arc shape was basically vertical downward. The weld pool flowed uniformly throughout the welding process (Fig. 5e–h).

The TW-GIA weld pool is mainly affected by the arc pressure P_a , the side wire droplet impact force F_d , the surface tension F_s , and the gravity F_g , as shown in Fig. 6. Gravity is vertically downward, and has no component in the opposite direction of welding. The component force P_{ax} of arc pressure in the opposite direction of welding can be expressed by Formula 1 [31]:

$$P_{ax} = P_a \cos \theta = \frac{\rho_g v_p^2}{2} \cos \theta \tag{1}$$

where ρ_g is the arc plasma density, θ is the angle between the arc and the base metal. v_p is the plasma velocity, which can be expressed by Formula 2 [31]:

Fig. 5 The flow process of the weld pool with welding angles of 35° and 65°



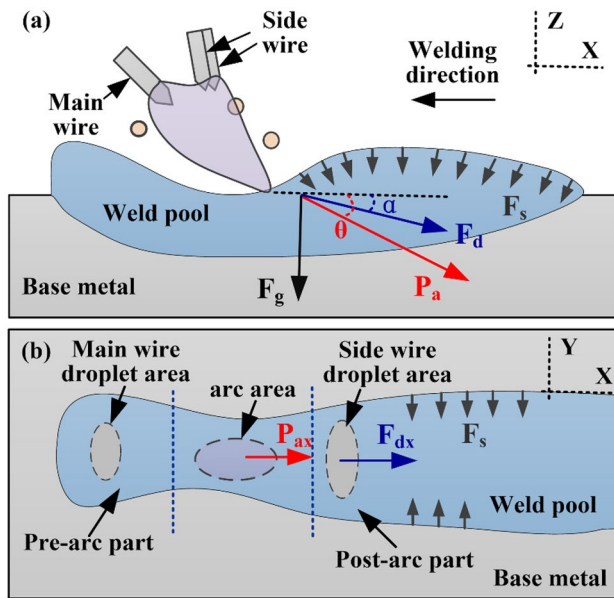


Fig. 6 Force diagram of TW-GIA weld pool: **a** front view, **b** top view

$$v_p = \sqrt{\frac{\mu I j}{2\pi \rho_g}} \quad (2)$$

where μ is the magnetic permeability, I is the welding current, and j is the plasma density where the arc is in contact with the weld pool. Therefore, the Formula 1 can be transformed into:

$$P_{ax} = \frac{\mu I j}{4\pi} \cos \theta \quad (3)$$

The adjustment of welding angle will not change the welding current and magnetic permeability. And according to the principle of minimum voltage, the minimum distance between three wires is preferentially selected as the arc conductive channel, so that the arc plasma density gradually decreases from the wires to the surrounding environment. The adjustment of the welding angle does not change the arc conduction path, nor does it affect the plasma density distribution characteristics. Therefore, under the condition that the welding height and welding current remain unchanged, the angle between the arc and the base metal is the decisive factor that affects the arc pressure. When the welding angle was 35° , the angle between the arc and the base metal (Fig. 5a) was significantly smaller than that of the welding angle was 65° (Fig. 5b). Therefore, according to Formula 3, it can be considered that the component of arc pressure in the opposite direction of welding increases with the decrease of welding angle.

The component of the side wire droplet impact force in the opposite direction of welding can be expressed by Formula 4 [32]:

$$F_{dx} = F_d \cos \alpha = \frac{4m_d v_d f}{\pi d^2} \cos \alpha \quad (4)$$

where m_d is the droplet mass, v_d is the droplet velocity, f is the droplet transfer frequency, d is the droplet diameter, and α is the angle between the droplet and the base metal. When the wire feeding speed and the welding speed are constant, only the angle between the droplet and the base metal is a variable in Formula 4. Therefore, similar to the arc force, the component of the droplet impact force in the opposite direction of the welding decreases as the angle between the droplet and the base metal increases.

Without considering the viscous force between the liquid metal and the base metal, the moving distance of the liquid metal before solidification can be expressed by Formula 5:

$$D = v_0 t + \frac{(P_{ax} + F_{dx})t^2}{2m} \quad (5)$$

where v_0 is the velocity vector in the opposite direction of welding when the weld pool is formed, t is the solidification time, and m is the quality of the liquid metal. It can be seen that the moving distance of the liquid metal is proportional to the combined force of the arc pressure and the droplet impact force. When the welding speed and wire feeding speed are unchanged, the quality of the liquid metal in the weld pool per unit time is constant. Combining the analysis of Formulas 3 and 4, it can be seen that the increase of the welding angle reduces the resultant force of the liquid metal flowing in the opposite direction of the welding, thereby shortening the flow distance of the liquid metal.

The difference in intermolecular attraction between liquid metal and air will produce surface tension, which is an obstacle to the spread of the liquid metal. It can be expressed by Formula 6 [33]:

$$F_s = F_s^o - A(T - T_m) - k \quad (6)$$

where F_s^o is the surface tension of the liquid metal at the melting point, A is the effective coefficient of surface tension, T is the temperature of the weld pool, T_m is the melting temperature of the metal, and k is the coefficient related to the degree of gas activity. It can be seen that the higher the temperature of the liquid metal, the lower the surface tension. The cooling rate of liquid metal can be expressed by Formula 7 [34]:

$$\varepsilon = \frac{2\alpha \Delta T}{\rho c \gamma} \quad (7)$$

where α is the heat transfer coefficient of liquid–solid interface, ΔT is the temperature difference between liquid metal and base metal, ρ is the density of liquid metal, c is the specific heat capacity of metal, and γ is the width of weld pool. When the welding angle is less than 45° , the liquid metal flows farther in the opposite direction of the welding, resulting in a larger distance from the arc. Since the thermal conductivity of the solid base metal is greater than that of air and liquid metal, a large temperature difference is formed between the base metal and the weld pool, resulting in an increase in the cooling rate of the liquid metal. When the welding angle is greater than 45° , the shortening of the distance between the liquid metal and the arc causes the temperature difference between the weld pool and the base metal to decrease, which reduces the cooling rate of the liquid metal. The advance rate of the liquid–solid interface is slowed so that the subsequent liquid metal is not hindered by the liquid–solid interface. In addition, the reduction of the distance between the main wire droplet and the side wire droplet results in a shortening of the convergence time of the two parts of the weld pool. It is beneficial for the pre-arc part of the weld pool to be filled to the void in front of the post-arc part of the weld pool in time.

In conclusion, the increase of welding angle can not only shorten the flow distance of liquid metal in the opposite direction of welding, but also promote the liquid metal to fill the void, which is beneficial to eliminate the humping bead.

3.3 The influence of welding height on humping bead

The TW-GIA arc conductive channel is established between the three wires, so changing the welding height will not affect the arc characteristics (arc temperature, stability, etc.) [17–20], but changes the contact range between the base metal and the arc. Figure 7 shows the appearance of butt welds with different welding heights. When the welding

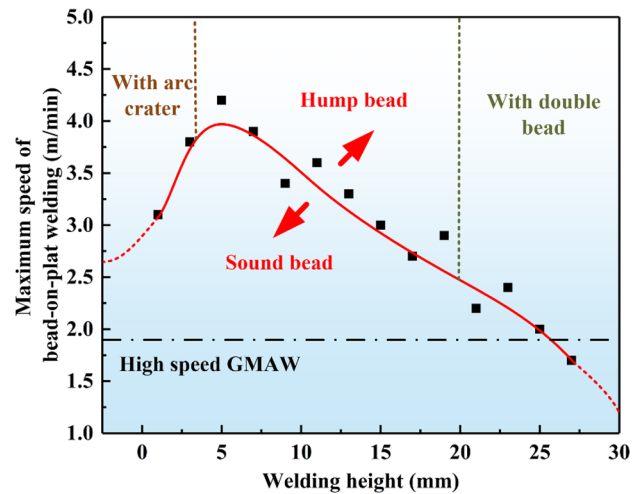


Fig. 8 The maximum welding speed of TW-GIA with different welding heights

height was 1 mm, periodic hump defects appeared in the weld bead, and a wave-shaped arc crater existed in front of the hump. When the welding height was 5 mm and 15 mm, the humped weld bead disappeared, and the weld seam was uniform. When the welding height was 25 mm, the humped weld reappeared, and the “double bead” defect appeared between the humps.

Figure 8 shows the maximum welding speed of bead-on-plate welding with different welding heights. The dotted line in the figure is the reported maximum speed of high-speed GMAW 1.77 m/min [35]. The maximum welding speed increases first and then decreases with the increase of welding height. The maximum welding speed is 4.2 m/min at a welding height of 5 mm, which is 137% higher than that of the high-speed GMAW welding. The humped weld bead with a welding height less than 3 mm is often accompanied by arc crater defects, and the humping bead with a height

Fig. 7 The appearance of butt welds with different welding heights: **a** welding height 1 mm, **b** welding height 5 mm, **c** welding height 15 mm, **d** welding height 25 mm

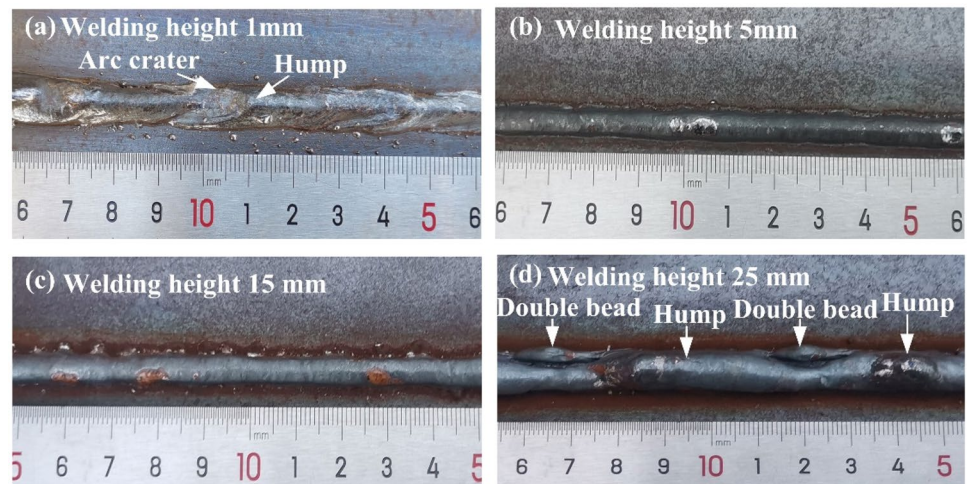
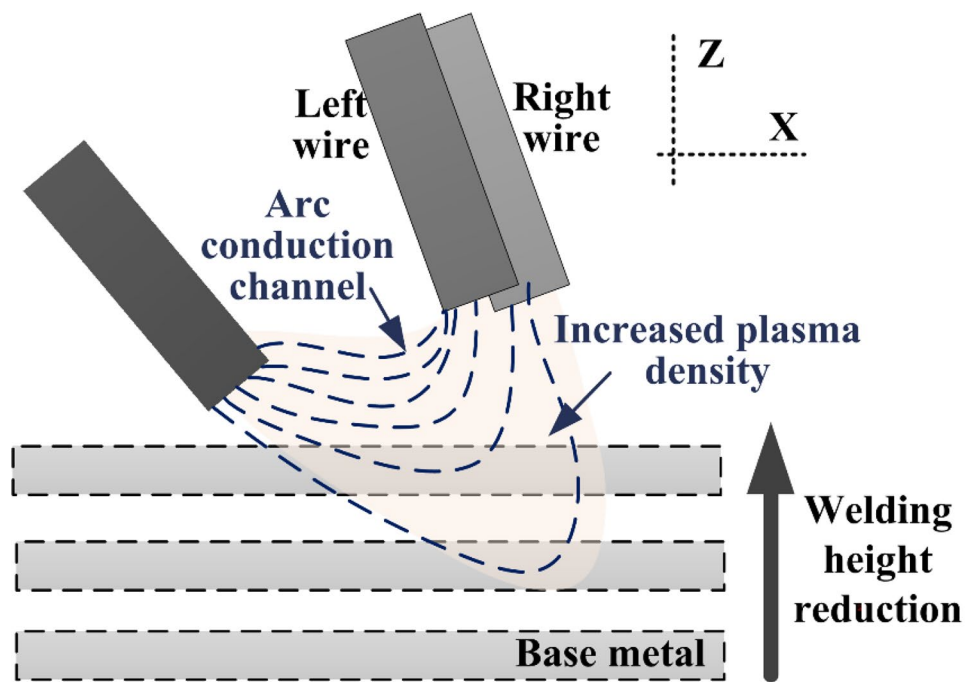


Fig. 9 Schematic diagram of the plasma conduction channel



greater than 20 mm is often accompanied by “double bead” defects.

Because the current forms a loop between the three wires, according to the principle of minimum voltage, the conductive channel is preferentially established at the shortest distance between the main wire and the two side wires. So in theory, the arc plasma density decreases with increasing distance from the wires. As shown in Fig. 9, as the welding height decreased, the closer the base metal was to the center of the conductive channel, the higher the plasma density at the point where it collides with the weld pool. This caused the arc pressure to increase as the welding height decreased. Therefore, it is considered that when the welding height is less than 3 mm, the strong arc pressure causes

a large-volume depression in the weld pool and pushes the liquid metal to flow rapidly behind the depression, resulting in metal accumulation. When the accumulated liquid metal is not fully spread and the subsequent liquid metal fail to fill the depression, the humping bead accompanied by the arc crater shown in Fig. 7a is caused.

The flow process of the weld pool with welding heights of 5 mm and 25 mm is shown in Fig. 10. When the welding height was 5 mm, the pre-arc part of the weld pool was generated under the convergence of the main wire droplets (Fig. 10a, b). In 639.2–644.7 ms, the liquid metal in the pre-arc part of the weld pool flowed in the opposite direction of the welding, and filled the depression to make the height of the weld uniform (Fig. 10c, d). When the welding height was

Fig. 10 Liquid metal flow process with the welding heights of 5 mm and 25 mm

Welding height	Welding current 320 A. Welding speed 3.2 m/min. Left/Right side wire feeding speed 5.8 m/min. Main wire feeding speed 8.7 m/min.			
	620.2 ms	622.2 ms	639.2 ms	644.7 ms
5 mm	(a)	(b)	(c)	(d)

increased to 25 mm, the weld pool was basically out of arc contact. In 309.2–412.2 ms (Fig. 10e, f), the pre-arc part and the post-arc part of the weld pool were formed separately. At 675.7 ms (Fig. 10g), the arc moved in the welding direction and passed through the pre-arc part. But the liquid metal did not flow, basically stayed in the original position, and gradually increased under the filling of the subsequent side wire droplets. The reason is that the base metal is almost completely out of the arc contact. According to Formula 5, the arc pressure was too small to cause the liquid metal to flow. The depression could not receive the filling of the liquid metal of the pre-arc part, and only the dripping of the side wire droplets, which caused it impossible to reach the height of the front and rear weld bead. When the arc completely passed through the pre-arc part (Fig. 10h), this part of the liquid metal was continuously filled with the side wire droplets, and the stack height was greater than that of the front and rear weld bead, resulting in the formation of the humping bead.

The “double bead” defect is caused by the special droplet transfer behavior of TW-GIA. Figure 11 shows the TW-GIA droplets transfer from a viewing angle parallel to the welding. The main wire droplets drips almost vertically, and the side wire droplets shows the characteristics of mutual repulsion transfer under the action of electromagnetic force [17]. The distance L between the droplets of the two side wires can be expressed by Formula 8:

$$L=2(v_y t + \frac{F_y t^2}{2m}) \tag{8}$$

where v_y is the velocity vector on the Y axis (parallel to the base metal) when the droplet leaves the wire, t is the transfer time, F_y is the resultant force in the Y axis direction at the moment the droplet leaves the wire, and m is the droplet mass. Among them, the transfer time t can be expressed by Formula 9:

$$t = \frac{\sqrt{v_z^2 + 2gH} - v_z}{g} \tag{9}$$

where v_z is the velocity vector on the Z axis (perpendicular to the base metal) when the droplet leaves the welding wire, g is the acceleration due to gravity, and H is the welding height. It can be seen from Formulas 8 and 9 that the droplet spacing of the two side wires increases with the increase of the welding height. When the welding height is less than 20 mm (Fig. 11b), although the droplets of the two side wires present a repulsive transfer, the transfer time is shorter and the distance between the droplets is smaller. In addition, the pre-arc part of the weld pool converged to the post-arc part, which contributes to the uniformity of the weld pool height. While the welding height is greater than 20 mm (Fig. 11c), the transfer time of the droplets is longer. As a result, the distance between the droplets of the wire is relatively long, and the droplets do not touch each other after reaching the base metal, and form two separate weld beads. According to the above analysis, the pre-arc part of the weld pool does not flow in the opposite direction of welding. When the side wire droplets cover the pre-arc part, the volume of the liquid metal increases and then rapidly solidifies to form a hump. Therefore, the droplets of the two side wires do not converge after reaching the base metal and nor be supplemented by the pre-arc part of the weld pool, resulting in the formation of “double bead” defects.

3.4 The influence of welding current on humping bead

In order to ensure the stability of the arc conductive channel, the distance between the anode and the cathode remains unchanged during the TW-GIA welding process. So, the change of welding current needs to be accompanied by the

Fig. 11 TW-GIA droplet transfer characteristics: **a** droplet transfer characteristics, **b** welding height less than 20 mm, **c** welding height greater than 20 mm

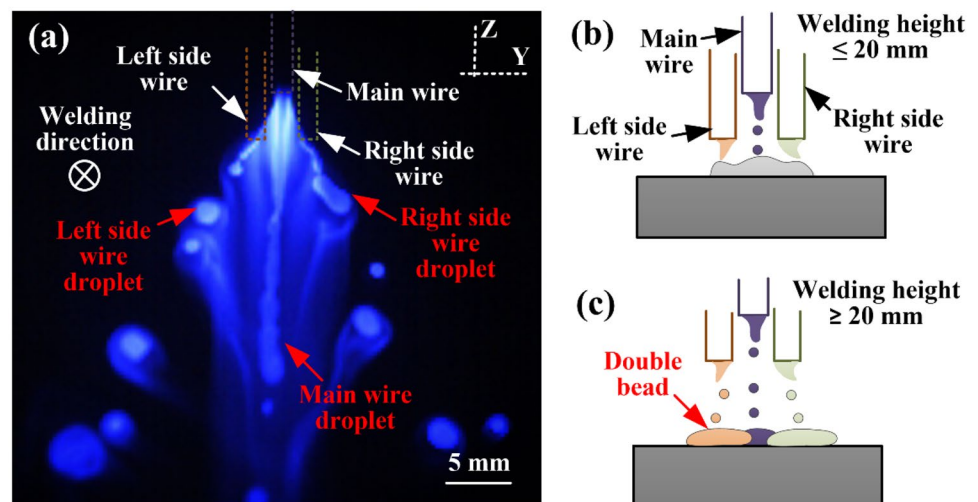


Table 2 Welding speed and wire feeding speed corresponding to welding current

Welding current (A)	280	320	360	400
Total wire feeding speed (m/min)	15.8	20.4	24.6	27.6
Welding speed (m/min)	1.58	2.04	2.46	2.76

change of wire feeding speed. In other words, each TW-GIA welding current of stable arc corresponds to an independent wire feeding speed. This means that if the TW-GIA welding speed is consistent and only the welding current is adjusted, the quality of the metal filled into the weld will be changed [36]. It is meaningless to analyze the influence of welding current on the humping bead under different metal filling qualities. Therefore, the ratio of the total wire feeding speed to the welding speed is set to a value of 10 to ensure the consistency of the filler metal quality, as shown in Formula 10:

$$\frac{(V_M + V_L + V_R)}{V_W} = 10 \quad (10)$$

where V_M is the main wire feeding speed, V_L is the left wire feeding speed, V_R is the right wire feeding speed, and V_W is the welding speed. The process parameters used are shown in Table 2.

The appearance of butt welds with different welding current is shown in Fig. 12. When the welding current was 280 A and 320 A, the welding bead was smooth and uniform. The appearance of the welding bead with a welding current of 360 A had slight hump, which can be considered as the critical current for the humping bead. Obvious hump appeared on the weld process with a welding current of 400 A. This indicates that when the quality of the filler metal remains unchanged, increasing the welding current will induce the formation of humping bead.

Due to the high-speed cameras are unable to capture the entire process of the weld pool far away from the arc under the interference of the arc's strong light, the infrared thermal

imaging system is used to detect the length of the liquid metal and the characteristics of the temperature field. The difference in reflectivity between solids and liquids makes it difficult to directly calibrate the molten pool temperature. So, the high temperature area above 1500 °C is collected as a similar-liquid metal area, and the high temperature profile is extracted, as shown in Fig. 13. The similar-liquid metal length increased from 3.3 to 9.4 mm with the welding current increased from 280 to 400 A. It can be considered that the length of the actual liquid metal also increased, which means that the distance between the liquid–solid interface of the weld pool and the arc increased. The temperature of the central axis of the weld within 5 mm behind the end of the similar-liquid area is collected, and the collection line ①②③④ are marked in Fig. 13. The temperature collection result is shown in Fig. 14. With the increase of welding current, the temperature gradient within 5 mm behind the similar-liquid area gradually increases.

As mentioned in Sect. 3.2, the hump is related to the accumulation of large volumes of liquid metal away from the arc and the excessive cooling rate. The arc is selected as the reference point, and the flow distance D of the liquid metal can be expressed by Formula 11:

$$D = (V_p + V_w)t \quad (11)$$

where V_p is the flow velocity of the liquid metal, V_w is the welding speed, and t is the flow time of the liquid metal. When the welding height is constant, the increase of welding current will increase the number of electrons and electron density at the collision of the weld pool. According to Formula 3, the increase in arc pressure leads to an increase in the reverse flow velocity of the liquid metal with the same metal filling quality. And according to Table 2, the welding speed increases with the increase of welding current. Therefore, the flow distance of the liquid metal increases with the increase of the welding current. The weld pool receives thermal energy transfer from the arc, and the further away from the

Fig. 12 TW-GIA butt weld appearance with different currents: **a** welding current 280 A, **b** welding current 320 A, **c** welding current 360 A, **d** welding current 400 A

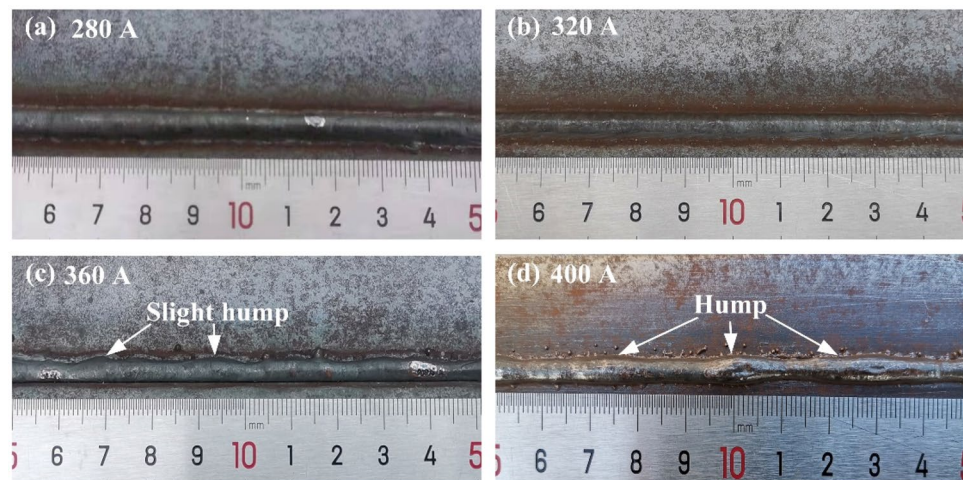
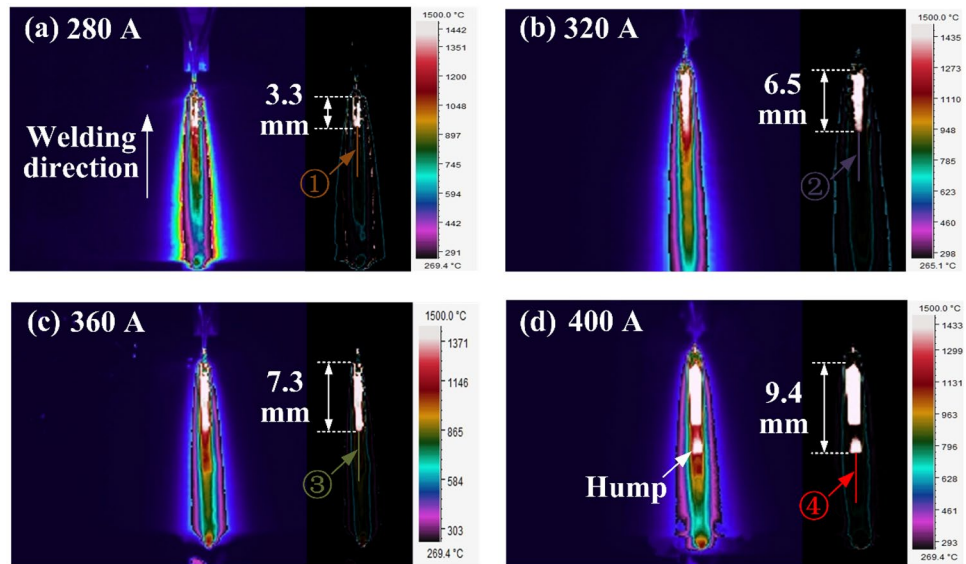


Fig. 13 Infrared thermal images with different welding current: **a** welding current 280 A, **b** welding current 320 A, **c** welding current 360 A, **d** welding current 400 A



arc the less thermal energy is received. Thereby, the temperature gradient behind the similar-liquid metal area decreases as the welding current increases, and the liquid metal solidifies faster (Formula 7). Based on the above analysis, when the welding current is less than 360 A, the liquid metal flows for a shorter distance under a smaller arc pressure, which causes the liquid–solid interface to be close to the arc so that the weld pool has sufficient liquid residence time. As a result, the weld pool can fully receive the subsequent filling of liquid metal to achieve a uniform weld height. While the welding current is greater than 360 A, due to the increase of the distance between the liquid–solid interface and the arc, the rapid solidification of the liquid metal hinders the subsequent filling of the liquid metal, resulting in inconsistency of the solidified metal in the weld and form a humping bead.

Of course, the critical current for humping bead is not constant, and it is affected by the ratio of total wire feeding speed to welding speed. Figure 15 shows the critical current of the humping bead-on-plate welding with different ratios. It can be seen that the critical current increases with the increase of the ratio. This indicates that the increase in the quality of the filler metal in the weld is beneficial to eliminate the humping bead. This is because when the ratio increases, according to Formula 5, the distance liquid metal moves in the opposite direction of welding becomes shorter. Which is beneficial to slow down the forward speed of the liquid–solid interface and promotes the spreading of liquid metal, so the critical current of the humping bead increases accordingly.

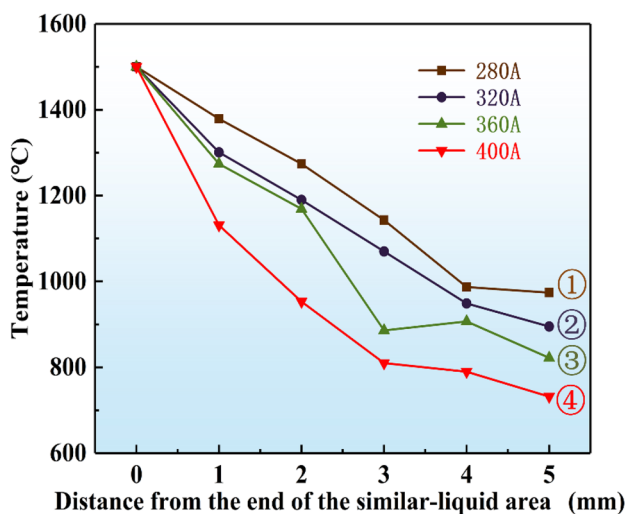


Fig. 14 Temperature distribution at the collection line

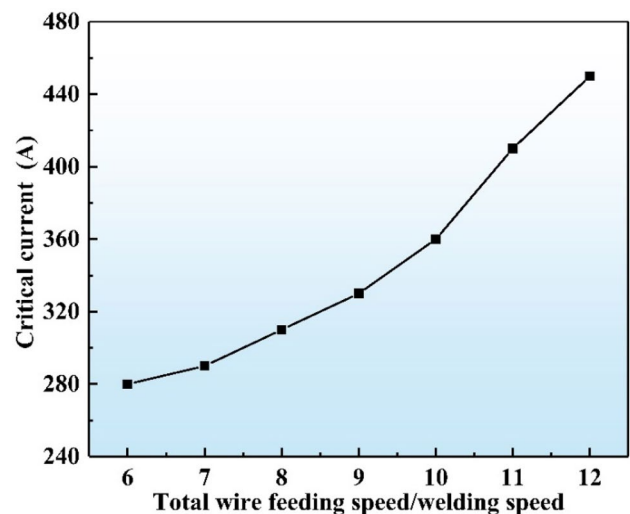


Fig. 15 Critical current with different ratios of total wire feeding speed to welding speed

4 Conclusion

In order to improve the welding efficiency of TW-GIA, the high-speed cameras and infrared thermal imaging system were used to characterize the formation mechanism of the humping bead during the high-speed TW-GIA welding process. The physical model was established to discuss the force mechanism of the weld pool, and the influence of the process parameters on the humping bead was studied. The conclusions are drawn as follows:

1. The arc pressure and droplet impact force in the opposite direction of welding decrease with the increase of welding angle, which can shorten the flow distance of liquid metal and is beneficial to eliminate the humping bead in TW-GIA.
2. The welding height that is too low will increase the arc pressure on the weld pool, resulting in the formation of the humping bead with arc craters. Too high welding height will increase the distance between the droplets of two side wires, and the pre-arc part of the pool cannot flow, leading to the humping bead with “double bead” defect. 3–20 mm is the achievable height range.
3. When the quality of the filler metal is consistent, the flow distance of liquid metal increases with the increase of the welding current, and the temperature gradient at the liquid–solid interface increases, which induced the formation of humping bead. When the ratio of the total wire feeding speed to the welding speed is 10, the critical current of the humping bead is 360 A, and the critical current increases as the ratio increases.
4. The maximum TW-GIA welding speed of bead-on-plate is 4.2 m/min, which is 137% higher than that of high-speed GMAW welding. The welding speed of butt weld with 3.8 mm thick plate can reach 2.46 m/min.

Author contribution Zeli Wang: conceptualization, methodology, writing-original draft, formal analysis. Tianyi Zhang: assist experiment, validation. Xiaonan Dong: conceptualization. Liming Liu: writing-review and editing, funding acquisition.

Funding This work was supported by the National Natural Science Foundation of China (No. 52175290).

Data availability All the data have been presented in the manuscript.

Declarations

Ethics approval The paper follows the guidelines of the Committee on Publication Ethics (COPE).

Consent to participate The authors declare that they all consent to participate this research.

Consent for publication The authors declare that they all consent to publish the manuscript.

Competing interests The authors declare no competing interests.

References

1. Bashkar R, Balasubramanian V, Mani C, Sonar T (2021) Establishing empirical relationship between welding current and weld metal deposition rate for submerged arc welding process. *Multi-scale and Multidisciplinary Modeling, Experiments and Design* 4:275–291
2. Wu DT, Zou Y, Zhao GL, Shi CW (2020) Wear-resistant surfacing layer prepared by high efficiency twin-wire indirect arc welding. *Mater Sci Forum* 985:229–239
3. Herawan SG, Rosli NA, Alkahari MR, Abdollah M, Ramli RF (2021) Review on effect of heat input for wire arc additive manufacturing process. *J Mater Res Technol* 11:2127–2145
4. Voiculescu I, Geanta V, Rusu C, Mircea O, Mistodie LR, Scutelnicu E (2016) Research on the metallurgical behaviour of X70 steel subjected to multi wire submerged arc welding. *Annals of the University Dunarea de Jos of Galati: Fascicle XI* 27:38–46
5. Wu KY, Zhan JT, Cao XW, Zeng M (2020) Metal transfer of aluminum alloy double-wire pulsed GMAW with a median waveform. *J Mater Process Tech* 286:1–116
6. Fang Y, Jiang X, Mo D, Zhu D, Luo Z (2019) A review on dissimilar metals' welding methods and mechanisms with interlayer. *Int J Adv Manuf Tech* 102:2845–2863
7. Lahnsteiner R (1992) T.I.M.E. process - an innovative MAG welding process. *Weld Rev Int* 11(1):17–20
8. Layus P, Kah P, Martikainen J, Gezha V, Bishokov R (2014) Multi-wire SAW of 640MPa arctic shipbuilding steel plates. *Int J Adv Manuf Tech* 75(5–8):771–782
9. Chen J, Zhang Y, Wu C, Padhy G (2019) Suppression of undercut defects in high-speed GMAW through a compound magnetic field. *J Mater Process Tech* 274:1–11
10. Lund H, Penttil S, Skriko T (2020) A knowledge-based multipass welding distortion estimation method for a multi-robot welding off-line programming and simulation software. *Procedia Manuf* 51:302–308
11. Huang J, Liu S, Yu S, An L, Yang F (2020) Cladding Inconel 625 on cast iron via bypass coupling micro-plasma arc welding. *J Manuf Process* 56:106–115
12. Miao YG, Xu XF, Wu BT, Li XX (2014) Effects of bypass current on the stability of weld pool during double sided arc welding. *J Mater Process Tech* 214(8):1590–1596
13. Li K, Zhang YM (2010) Interval model control of consumable double-electrode gas metal arc welding process. *IEEE T Autom Sci Eng* 7(4):826–839
14. An Q, Wen YX, Matsuda J, Xu JY, Wu DT, Zou Y (2021) Corrosion resistance and high temperature wear behavior of carbide-enhanced austenite-based surfacing layer prepared by twin-wire indirect arc welding. *Mater Res Express* 8:1–11
15. Shi C, Zou Y, Zou Z, Wu DT (2014) Twin-wire indirect arc welding by modeling and experiment. *J Mater Process Tech* 214(11):2292–2299
16. Wu DT, Hu C, Zhao W, Zhang YG, Zou Y (2019) Influence of external magnetic field on twin-wire indirect arc surfacing stainless steel layer. *Vacuum* 169:1–7
17. Fang DS, Song G, Liu LM (2016) A novel method of triple-wire gas indirect arc welding. *Mater Manuf Process* 31(3):352–358

18. Liu LM, Yu SB, Hu CH (2019) Analysis of arc shape and weld forming in triple-wire indirect arc welding. *Transactions of the China Welding Institution* 40(6):1–6
19. Liu L, Yu SB, Song G, Hu CH (2019) Analysis of arc stability and bead forming with high-speed TW-GIA welding. *J Manuf Process* 46:67–76
20. Liu LM, Hu CH, Yu SB, Song G (2019) A triple-wire indirect arc welding method with high melting efficiency of base metal. *J Manuf Process* 44:252–260
21. Wang L, Wu C S, Chen J, Gao J, Hu Q (2020) Experimental measurement of fluid flow in high-speed GMAW assisted by transverse magnetic field. *J Manuf Process* 56(A):1193–1200
22. Nguyen TC, Weckman DC, Johnson DA (2005) The humping phenomenon during high speed gas metal arc welding. *Sci Technol Weld Join* 10:447–459
23. Zähr J, Füssel U, Hertel M, Lohse M, Schnick M (2012) Numerical and experimental studies of the influence of process gases in TIG welding. *Weld World* 56(3–4):85–92
24. Li KH, Chen JS, Zhang YM (2007) Double-electrode GMAW process and control. *Welding J* 86(8):231–237
25. Kanemaru S, Sasaki T, Sato T, Tanaka M, Kanemaru S, Mishima H (2014) Study for TIG-MIG hybrid weld process. *Weld World* 58(1):11–18
26. Shoichi M, Yukio M, Koki T, Yasushi T, Yukinori M, Yusuke M (2013) Study on the application for electromagnetic controlled weld pool welding process in overhead and flat position welding. *Sci Technol Weld Join* 18:38–44
27. Wu CS, Yang F, Gao J (2016) Effect of external magnetic field on weld pool flow conditions in high-speed gas metal arc welding. *Proc Inst Mech Eng Part B J Eng Manuf* 230:88–93
28. Wang L, Wu CS, Gao JQ (2016) Suppression of humping bead in high speed GMAW with external magnetic field. *Sci Technol Weld Join* 21:131–139
29. Gatzen M, Tang Z, Vollertsen F (2011) Effect of electromagnetic stirring on the element distribution in laser beam welding of aluminium with filler wire. *Phys Procedia* 12:56–65
30. Bachmann M, Avilov V, Gumenyuk A, Rethmeier M (2014) Experimental and numerical investigation of an electromagnetic weld pool support system for high power laser beam welding of austenitic stainless steel. *J Mater Process Technol* 214:578–591
31. Xu XK, Yang HY, Liu LM (2021) Study on time characteristics of coupling discharge in pulsed laser induced double-TIG welding. *Int J Adv Manuf Tech.* <https://doi.org/10.21203/rs.3.rs-796847/v1>
32. Zhang RZ, Zhang B, Lv Q, Li J, Guo P (2019) Effects of droplet shape on impact force of low-speed droplets colliding with solid surface. *Exp Fluids* 60(4):60–64
33. Lu SP, Fujii H, Nogi K (2008) Marangoni convection and weld shape variations in He–CO₂ shielded gas tungsten arc welding on SUS304 stainless steel. *J Mater Sci Technol* 43(13):4583–4591
34. Wang ZJ (2007) Fusion welding method and equipment. Machinery Industry Press, Beijing (in Chinese)
35. Wang L, Chen J, Wu C, Gao J (2016) Backward flowing molten metal in weld pool and its influence on humping bead in high-speed GMAW. *J Mater Process Technol* 237:342–350
36. Yu SB, Liu ZH, Shi T, Guo JH, Liu LM (2021) Effect of wire feeding speed on the stability and weld formation of triple-wire indirect arc welding. *Weld Technol* 50(1):35–39

Publisher's Note Springer Nature remains neutral with regard to jurisdictional claims in published maps and institutional affiliations.

Springer Nature or its licensor holds exclusive rights to this article under a publishing agreement with the author(s) or other rightsholder(s); author self-archiving of the accepted manuscript version of this article is solely governed by the terms of such publishing agreement and applicable law.